# A tool to estimate factor of safety for varying slope height and angle in specific rock mass conditions

**Styles, T. D.** *Mining One Consultants, Ashbourne, UK*

**Jackson, S. J.** *Mining One Consultants, Cornwall, UK*

**Vakili, A.** *Mining One Consultants, Melbourne, Australia*

## Abstract

*The presentation of slope angle versus slope height is a useful and quick-to-use tool. This can be used to either provide an initial guide for slope design or as a reference to study the influence of inputs on analysis results. The current approaches that are available are either complex, generic or cannot be equated to the rock mass classification approach that is routinely used in modern rock mechanics. This paper presents an approach, based on advanced numerical modelling, which defines the factor of safety (FS) of specific slope height and slope angles for prescribed conditions. Several charts are presented, referred to as 'Slope Stability Curves', which demonstrate the impact of overall slope height and angle, on the FS. The approach provides the means to study how key aspects affect slope stability. By comparing the current curves, the influence of rock mass strength and groundwater on slope stability can be quantified.*

## 1 Introduction

In the efforts of achieving an economically viable mine, geotechnical guidance for slope design is often pushed to provide slope angles that are as steep as possible, especially during early stages of a project (scoping/pre-feasibility studies). With the ever-increasing depths to which open pit mines are developing, it is paramount that the slope design is safe, realistic and achievable. The approach suggested in this paper, provides guidance for the design of inter-ramp and overall slopes, with a method to develop recommended slope angles for slope heights within specified rock mass conditions.

The approach, which was first introduced in Styles and Vakili (2020), uses an advanced numerical modelling technique, which has enabled the simulation of numerous slope height and angle combinations, resolving the factor of safety (FS), for a number of case study rock masses. The output is a chart of slope angle versus slope height, which is intended to be a quick and easy-to-use tool, providing a guide for slope design or a basis for studying the influence of model inputs.

Examples are given with different rock mass strength criteria and with groundwater, as a proof of concept. In time, it is intended that further rock mass conditions will be analysed, and a database of 'Slope Stability Curves' could be developed. The approach can also be automated, to provide an opportunity to input specific rock mass conditions, and for Slope Stability Curves to be developed automatically via cloud computing on 3D models. In addition, future efforts may also entail the incorporation of the suggested slope parameters into mine planning software, allowing the optimisation of slope angle for each stage of a pit.

## 2 Existing Approaches

There are a number of slope angle versus slope height graphs available in literature. It must be recognised that some are designed to generic, whilst others offer an insight into the variability of stability for different rock mass conditions. Two of the most well-known charts are presented in Hoek and Bray (1981) and Sjöberg (1999). As shown in Figure 1a, Hoek and Bray (1981) developed their chart on stable and unstable slopes that had been observed in Spain. The Hoek and Bray (1981) chart is for a variety of rock mass conditions and therefore is considered to be 'generic'. To illustrate the potential variability, an example from Kanmantoo Copper Mine is plotted on Figure 1b. The Hoek and Bray (1981) chart suggest that this slope should have failed, whereas a calibrated analysis presented by Lucas at al. (2020) suggest that the FS is 1.4.

Sjöberg (1999) provided a chart that indicated the ISRM qualitative rock strength for each case study, to provide an insight into specific rock mass conditions. Haines and Terbrugge (1991) classified the stability based on MRMR, this is useful way of understanding variability with differing rock mass strength. However, both their chart and the Hoek and Bray chart (Figure 1), are limited to a slope height of 300 m. Carter (2018) presented a database of empirical examples for slopes up to 1,500 m. In addition, the conditions are classified using the Hoek-Brown constant, $m_b$, which is beneficial considering that the Hoek-Brown strength criterion is currently the most favoured approach to representing rock mass strength.

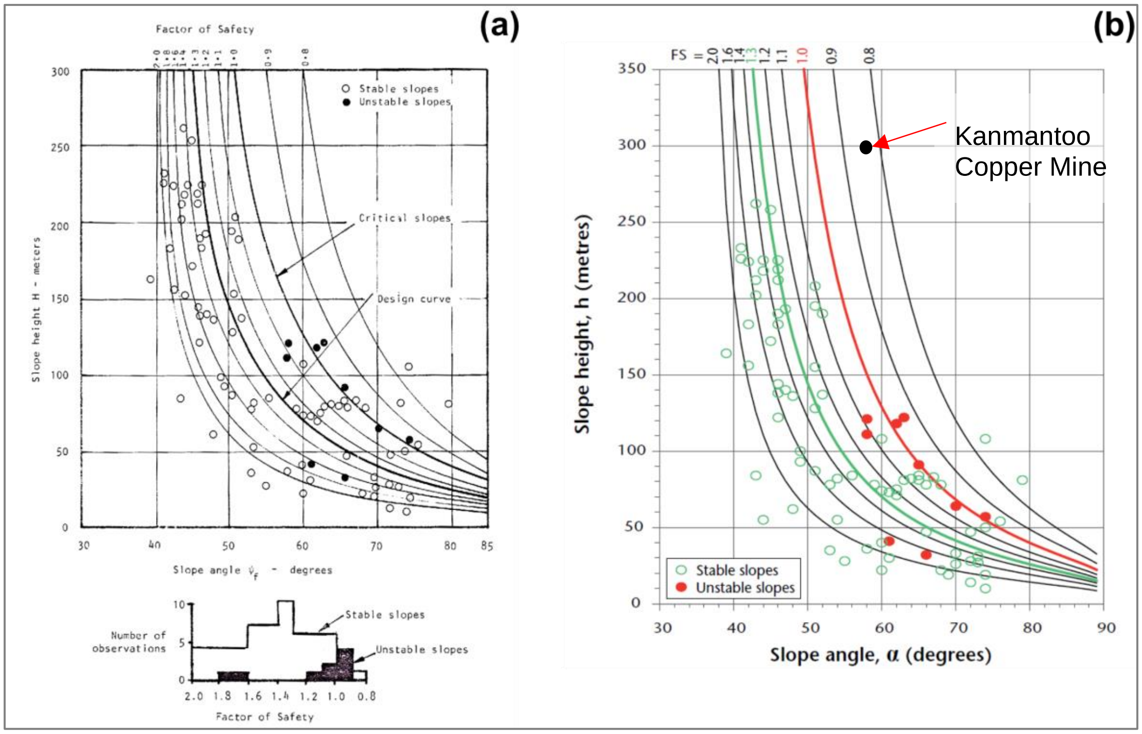


Figure 1. (a) Slope angle versus slope height chart with for FS best fit lines, for porphyry slopes in the Rio Tinto area, Spain (after Hoek and Bray, 1981), (b) the reproduced coloured version of the chart presented in Read and Stacey (2009) with an additional data point from a recent analysis of the Kanmantoo Copper Mine

The above charts were based on case study slopes. Another way to develop charts it to use numerical modelling, which provides the means to test numerous iterations. Carranza-Torres and Hormazábal (2018 and 2020), have developed several Microsoft Excel workbooks. The Excel workbooks take the results from limit equilibrium (LE) analyses. Subsequently, the FS for a slope geometry is interpolated, based on a material strength that is defined by the user. Initially in 2018, an Excel sheet was provided in which a material with a Mohr-Coulomb strength can be defined, as documented in Carranza-Torres and Hormazábal (2018). An additional sheet was provided in Carranza-Torres and Hormazábal (2020), allowing Hoek–Brown inputs to be defined.

Li et al. (2008) also used a numerical modelling approach, analysing a range of slopes in both LE and finite element (FE) analysis, resulting in a series of charts that can be used to estimate FS for slopes based on GSI and Hoek Brown strength parameters. As reported by Li et al. (2008) the results have the same limitations as the Hoek-Brown criterion from which they are established. The application of a complete constitutive model such as the Improved unified Constitutive Model (IUCM), introduced in Vakili (2016), provides a solution to many of the limitations.

Sun et al. (2016) and Wei et al. (2021) have expanded on the work by Li et al. (2008), completing FE analysis to develop slope stability charts for the estimation of FS. Wei et al. (2021) approach involves calculating a critical failure strength by adjusting material parameters (UCS, GSI, $m_i$, and D). Slope configurations of varying angle and height were analysed up to 80$^o$ and 100 m, the rock mass density was fixed at a constant 2500 kg/m$^3$.

It is suggested that all stability chart approaches intend to provide a reference that enables estimate stability. The approach presented herein, is intended to demonstrate a proof of concept by which slope stability charts can be developed rapidly, for specific rock mass conditions and slope configurations.

# 3 Proposed Approach

As discussed briefly in Section 1, a chart of slope angle versus slope height is resolved in the proposed approach. The chart referred to as a ‘Slope Stability Curve’ comprises of four lines, each of which provides the relationship for slope height and angle at a specific FS. Although any FS can be plotted onto the chart, four FS have been chosen (Table 1) based on the criteria suggested by Priest and Brown (1983). Read and Stacey (2009) state the categories suggested by Priest and Brown (1983), to be conservative. However, it is recommended that a level of conservatism is applied, until further complexity (for instance anisotropy), is introduced.

The area above the respective FS is coloured to provide a rapid view of the slope geometries that have lower safety factors. To create the curves the following method is used:

1. Two-dimensional slope geometries are developed following the current approach. As discussed in Section 1, in the future, Slope Stability Curves can be developed automatically via cloud computing on 3D models. Typically, a minimum of four different slope angles and six slope heights are required to provide an adequate coverage of the FS, as illustrated in Table 2 (this results in a minimum of 24 models, with ideally ≥4 results required in each category of stability, which is defined by the consequence of failure).

2. The geometries are read into SlopeX, which was is introduced in detail in Vakili et al. (2020). In summary SlopeX is a tool that both streamlines advanced numerical modelling and provides accurate results. It is developed by Cavroc and uses FLAC3D (the finite difference code developed by Itasca), to automatically create an optimised mesh that meets the required discretization for establishing an accurate estimation of FS for a rock slope. A simulation-ready input file is made in minutes, and the input file can be replicated and modified in seconds, allowing the models to be setup rapidly and efficiently. A critical part of the method is the use of the ‘Improved Unified Constitutive Model’, introduced initially by Vakili (2016) and integrated within SlopeX. By using IUCM, stress relaxation is explicitly simulated by a realistic strain-softening formulation. This results in a solution that is less reliant on the disturbance factor (‘D’), which is required in the Hoek-Brown strength criterion.

3. SlopeX has an automated shear strength reduction process which can be used to derive the FS of the stability analyses within the matrix (Table 2). Once the FS of each iteration has been resolved, a chart of FS for each slope angle is produced. Equation [1] is the power curve that describes the relationship between FS and slope height (h) for each slope angle. A, B and C are constants, which are generated for each slope angle.

$$FS = Ae^{-Bh} + C \qquad [1]$$

4. Equation 1 is re-arranged as shown in Equation [2], to determine the slope height for a specific FS. Subsequently a plot is created of slope height, using the constants A, B and C that were defined for each slope angle during Step 3. This allows the FS design line to be plotted onto a slope height versus slope angle chart. Note that the relationship for a FS of 1 can be problematic to attain due to the difficulty solving $\log_e$ when the FS is 1; therefore, it may have to be inferred using the data points. The collection of these design lines is referred to as a ‘Slope Stability Curve’, which is applicable for the inputs that were used for the models in the matrix. Each curve reflects the anticipated FS for different slope geometries.

$$h = \frac{\log_e(FS-C)/A}{-B} \qquad [2]$$

5. As a final stage to confirm the constants that were derived in Step 3, the result from each model is plotted onto the slope height versus slope angle chart. If any of the curves appear to provide a poor fit to the FS results from Step 3, then further models are added into the matrix, to improve the design curve.

To implement groundwater within the process described above, similar groundwater conditions need to be assumed for different slope heights and slope angles. The circular failure charts which Hoek and Bray (1981) developed, used an approach in which groundwater conditions were assumed from associated images. The same groundwater assumptions are applied for this work, as presented in Figure 2.

Table 1. Slope height versus slope angle formulations that are presented on a 'Slope Stability Curve', are based on the FS acceptance criteria from Priest and Brown (1983).

| FS | Suitable for: | Consequence of Failure |
|---|---|---|
| 1.0 | - | - |
| 1.3 | Temporary slopes, not adjacent to haulage roads | Not Serious |
| 1.6 | Any slope of a permanent or semi-permanent nature | Moderately Serious |
| 2.0 | Critical permanent slopes carrying major haulage roads or underlying permanent mine installations | Very Serious |

Table 2. Matrix of stability analyses, which form the basis for the slope stability curves; increments of slope angles and slope heights are provided as an example for an analysis of overall slope stability in a relatively strong rock mass.

| | | Slope Angle | | | |
|---|---|---|---|---|---|
| | | Ψ | Ψ + 5° | Ψ + 10° | Ψ + 15° |
| Slope Height | h | FS ≥2.0 | FS ≥2 | FS ≥2 | FS ≥1.6 |
| | h + 100 m | FS ≥2.0 | FS ≥1.6 | FS ≥1.6 | FS ≥1.3 |
| | h + 200 m | FS ≥1.6 | FS ≥1.6 | FS ≥1.3 | FS ≥1.3 |
| | h + 300 m | FS ≥1.6 | FS ≥1.3 | FS ≥1.3 | FS ≤1.0 |
| | h + 400 m | FS ≥1.3 | FS ≥1.3 | FS ≤1.0 | FS ≤1.0 |
| | h + 500 m | FS ≥1.3 | FS ≤1.0 | FS ≤1.0 | FS ≤1.0 |

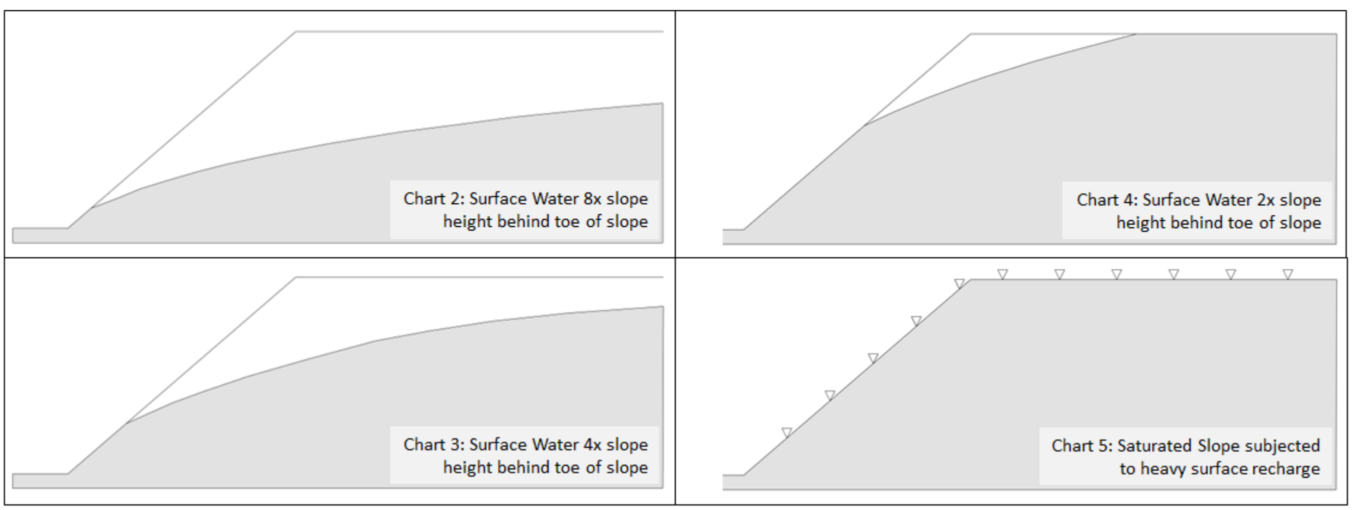


Figure 2. Phreatic surfaces that are applied in the current approach (after Hoek and Bray, 1981), note that Chart 1 represents fully drained conditions and is subsequently not shown.

## 4 Examples

As part of this work, two rock masses have been analysed. Rock Mass A can be considered as a moderate rock mass with a 'very blocky' structure and 'fair' surface conditions. This was chosen to represent typical moderate conditions which are experienced often in rock masses. Styles and Vakili (2020), presented an analysis of drained conditions in Rock Mass A, along with two other rock masses (Rock Mass B and C).

Rock Mass D is also introduced in this work, which is a soft rock that was experienced at a mine site in Australia, where a volcanic rock mass has been completely weathered. Table 3 presents the strength inputs for both Rock Masses A and D. Note that in all cases a simple in-situ stress has been assumed, where there is equality between the horizontal stresses and the vertical stress.

With the analysis continuing from the previous work, FLAC3D v5 was used to resolve the curves for Rock Mass A. Rock Mass D is a more recent addition to the project, therefore the analysis has been resolved using FLAC3D v7. Some comparisons have been completed between v5 and v7 of FLAC3D, with the FS being ~0.05 lower in the latter. This is assumed to be due to changes in the solver, and it is a change that is low enough to be considered acceptable. It is the authors belief, that in the mining industry, there is rarely sufficient confidence in geotechnical parameters to consider FS in increments of <0.05.

Table 3. Material strengths applied during the analyses for both Rock Masses A and D.

| Parameter | | | Rock Mass A | Rock Mass D |
|---|---|---|---|---|
| **Common inputs** | Density | $\rho$ (t/m$^3$) | 2.70 | 1.95 |
| | Young's Modulus | $E$ (GPa) | 30 | 0.075 |
| | Poisson's Ratio | $\nu$ | Calculated using GSI | 0.35 |
| **IUCM** | Geological Strength Index | GSI | 50 | - |
| | Hoek Brown Constant | $m_i$ | 16 | - |
| | Intact compressive strength | $\sigma_c$ (MPa) | 50 | - |
| **Mohr-Coulomb** | Cohesion | c (kPa) | - | 26 |
| | Friction | $\Phi$ (°) | - | 27 |
| | Tension | $\sigma_t$ (kPa) | - | 1 |
| | Dilation Angle | $\Psi$ (°) | - | 5 |
| **Residual Strength** | Cohesion | $c_{res}$ (kPa) | 0 | - |
| | Friction | $\Phi_{res}$ (°) | 38 | - |
| | Tension | $\sigma_{t\ res}$ (kPa) | 0 | - |
| | Critical Reduction Factor[1] | CritRed | 1 | - |

[1] With the Critical Reduction Factor set at a value of 1, the level of plastic strain at which the rock mass reduces to residual strength is automatically calculated based on GSI value and the zone size (see Vakili, 2016).

### 4.1 Results for Rock Mass A

The Slope Stability Curve for Rock Mass A was originally presented in Styles and Vakili (2020). However, as discussed at the time, further analysis was required to refine the relationship for a FS 1.6. Although further work was completed with the revised chart presented in Figure 3, additional results with a FS of between 1.3 and 1.6 are required. This reiterates the need to satisfy the matrix that was presented in Table 2; in this case >4 results are required to define the FS of 1.3 on the Slope Stability Curve. Analyses with groundwater have been completed using a more focussed set of slope geometries that satisfies the matrix, with a groundwater condition that follows Chart 4 (Figure 2). The Slope Stability Curve with groundwater is presented in Figure 4.

When Figures 3 and 4 are compared, it can be appreciated that the FS decreases significantly when groundwater is introduced. Furthermore, the FS would be lower if other critical characteristics, such as anisotropy are introduced. As an example, the FS was analysed for a fully drained 300 m high slope with a slope angle of 50° and the anisotropic properties listed in Table 4. It was found that the FS decreases by a value of ~1 once anisotropy was included (Figure 5). There would be a further decrease if groundwater was introduced; future analyses will include both anisotropy and groundwater.

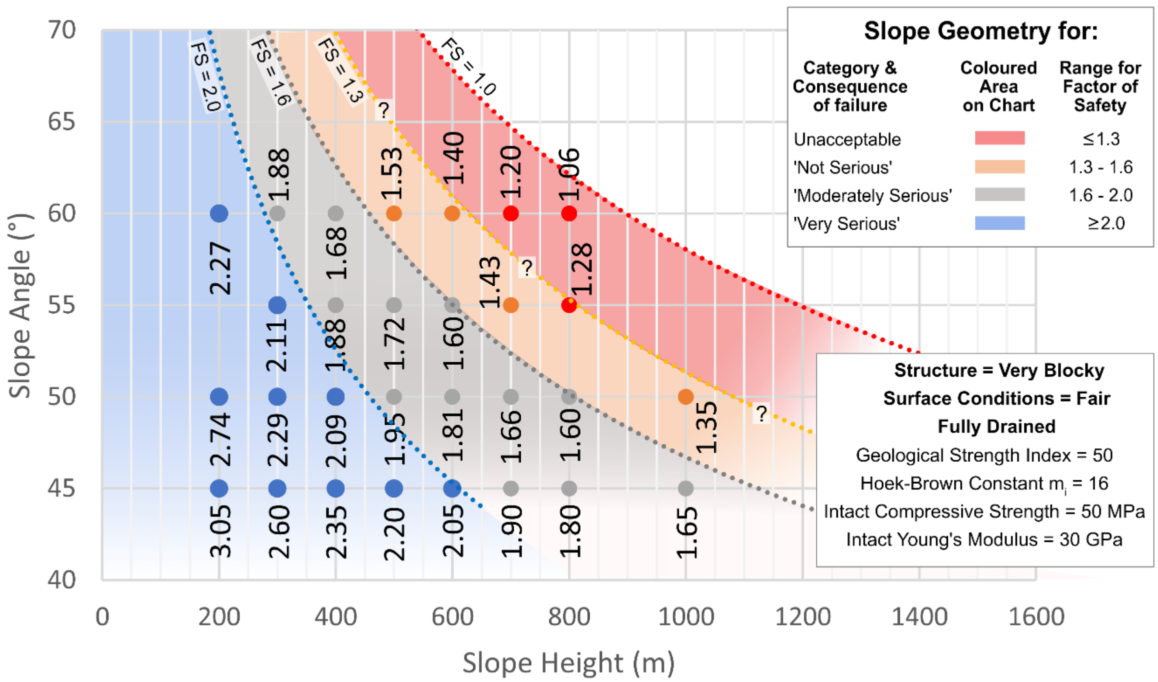


Figure 3. Slope Stability Curve for Rock Mass A in a fully drained scenario (further analysis is suggested to improve the limits suggested for the FS of 1.3 and 1 curves), FS results from the models used to create the curves are labelled.

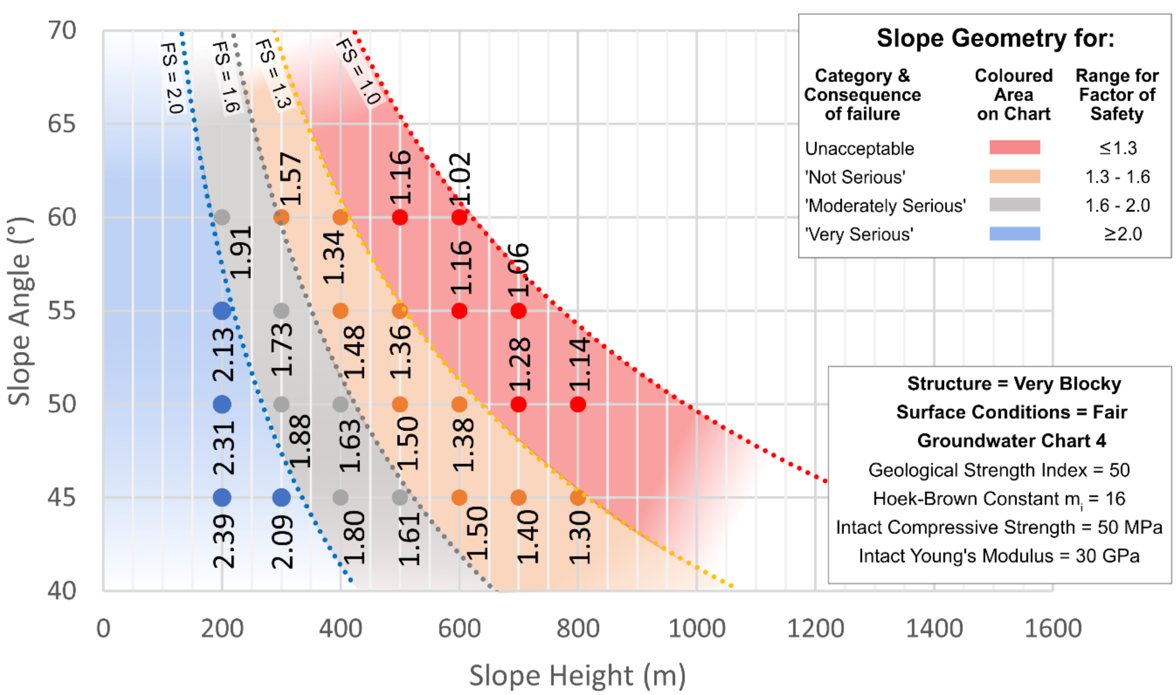


Figure 4. Slope Stability Curve for Rock Mass A with groundwater chart 4, the FS results from the models used to create the curves are labelled.

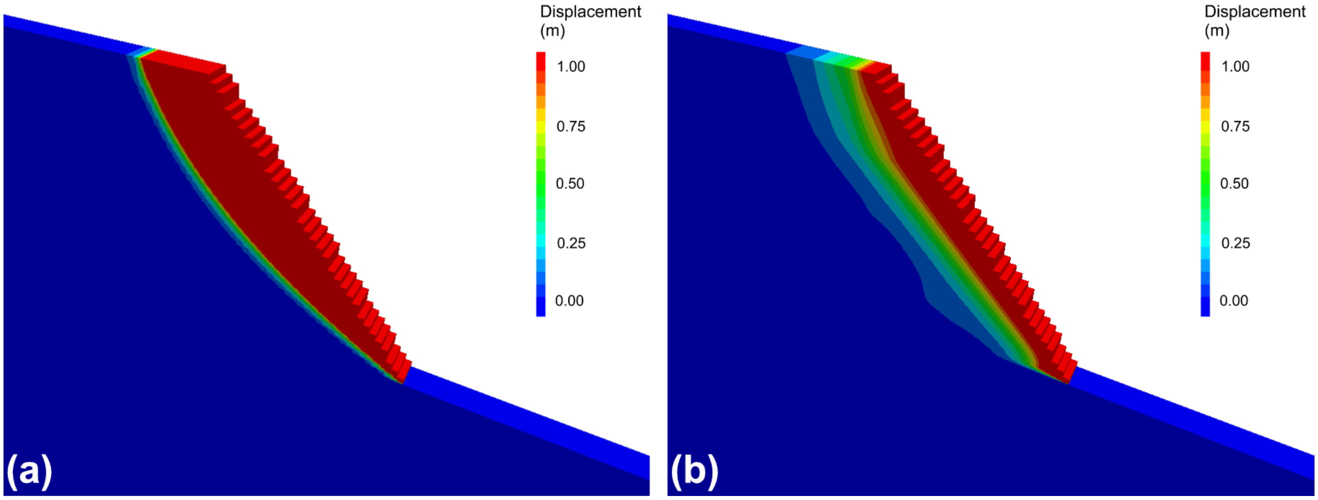


Figure 5. 300 m high slope with a slope angle of 50° in Rock Mass A, (a) showing displacement at the FS of 2.29 in an isotropic model, (b) anisotropic model with subsequent decrease in FS to 1.28 and decrease in the depth of displacement.

Table 4. Inputs used for an example anisotropic analysis, in Rock Mass A.

| Parameter | Value |
|---|---|
| Dip of anisotropy (°) | 45 |
| Direction | Out of slope |
| $m_i$ in direction of anisotropy | 8 |
| Anisotropic Factor ($\sigma_c$ max. / $\sigma_c$ min.) | 3 |

With the slope stability curves defined, it is possible to estimate the slope angle for different slope heights at a desired FS. As an example, Table 5 lists the slope angles for a 500 m slope in Rock Mass A. The influence of groundwater can be rapidly plotted. In general, Figure 6 illustrates that the reduction in FS due to groundwater, decreases as slope height increases. However, above a slope angle of 50° and below a slope height of 300 m there is complex behaviour, where the reduction in FS due to groundwater is lower than would be anticipated.

Table 5. Example to illustrate the slope angles for different 'categories' of slope for Rock Mass A, the result for a FS of 1.3 in a fully drained scenario, has not been included as it is suggested that the slope stability curve is improved.

| Classification of Slope | Suggested Slope Angle for Specified Groundwater | |
|---|---|---|
| | Chart 1 (fully drained) | Chart 4 |
| Critical slope (desired FS = 2) | 49° | 37° |
| Permanent/semi-permanent slope (desired FS = 1.6) | 58° | 46° |
| Temporary slope (desired FS = 1.3) | 67° | 55° |
| Slope failure (FS = 1) | 72° | 66° |

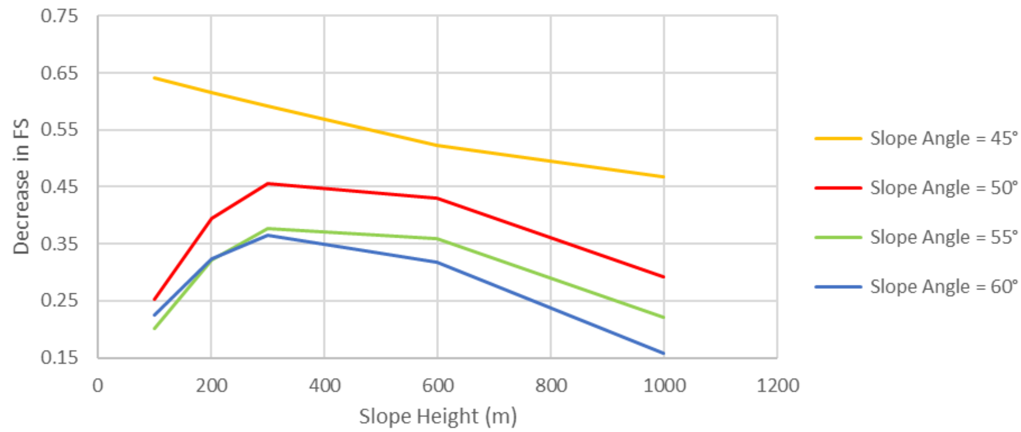


Figure 6. Influence of groundwater in Rock Mass A, expressed as the difference in FS between the Slope Stability Curves from Chart 1 (fully drained) and Chart 4.

As discussed in Section 2, Carranza-Torres and Hormazábal (2020) provided an LE-based Excel solution. This provides a rapid means of comparison to the results from this analysis. Figure 7 illustrates that the Slope Stability Curves consistently suggests a slightly higher FS at lower slope heights, than the LE-based solution. However, at slope heights greater than approximately 500 m, the Slope Stability Curve suggests a significantly lower FS. This is likely to be a result of the 'missing physics' in LE, as suggested by Lorig (2022) LE-based methods use the summation of moments, horizontal forces and vertical forces, to resolve static equilibrium, it does not analyse strains and displacements. As discussed above, complex behaviour, exists in low slope heights with steep angles, and at greater slope heights the influence of stress at the toe of the slope is not considered in a LE-based solution.

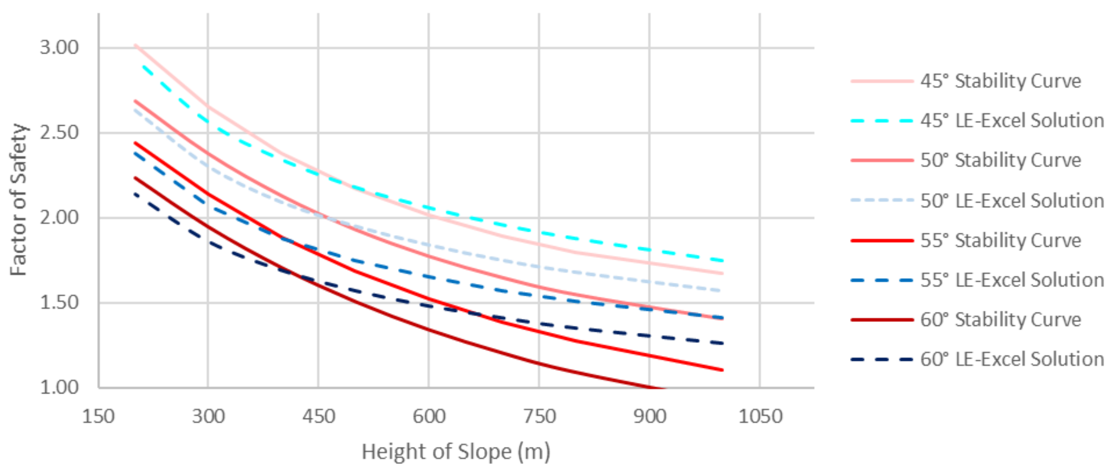


Figure 7. Comparison of Slope Stability curves for Rock Mass A (fully drained), with the LE-based Excel solution from Carranza-Torres and Hormazábal (2020).

## 4.2 Results for Rock Mass D

As previously stated, Rock Mass D is a weathered material therefore the slope heights and angles that have been analysed are considerably lower than in Rock Mass A. Figures 8 and 9 present the Slope Stability curves for both a drained condition, and with a groundwater chart that represents a semi-drained state.

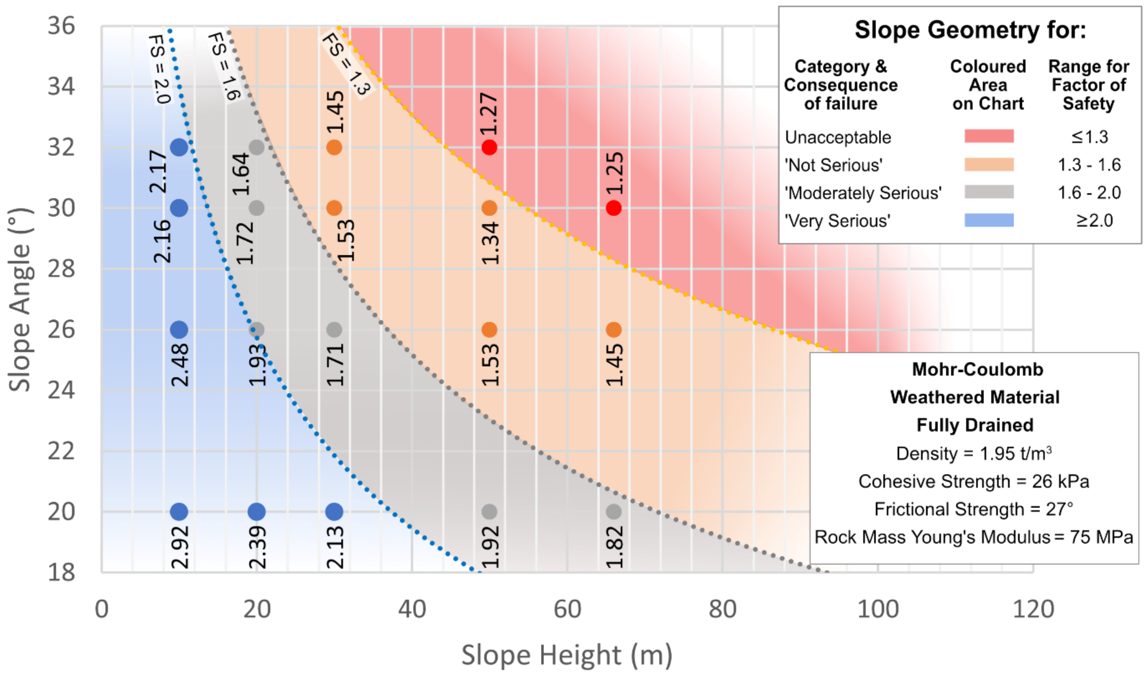


Figure 8. Slope Stability Curve for Rock Mass D in a fully drained scenario (design curves for FS of 1.0 has not been plotted due to issues discussed in Step 4 of Section 3), the FS values are labelled on each point.

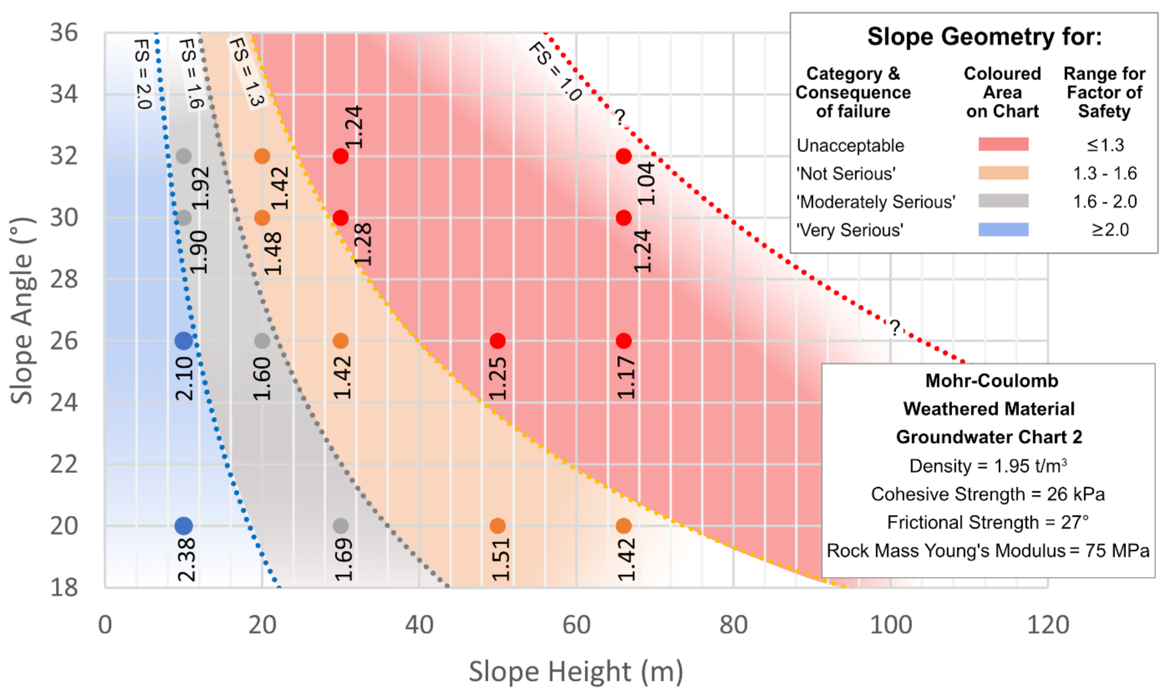


Figure 9. Slope Stability Curve for Rock Mass D with groundwater chart 2 (design curve for FS of 1.0 is inferred), the FS values are labelled on each point.

With the slope stability curves defined, as discussed in Section 4.1, it is possible to interpret the influence of groundwater. In general, for Rock Mass D, the influence of groundwater decreases as slope height and slope angle increases. In the case of Rock Mass D, the matrix of analyses that form the basis for the slope stability curves, has been analysed with sufficient coverage of the different categories of FS. Subsequently, a full chart can be produced showing the decrease in slope angle for a desired FS, which is necessary once groundwater is introduced into the slope.

As illustrated in Figure 10, with an increase in slope height there is an increase in the reduction of slope angle that is necessary due to groundwater, as the desired FS of a slope increases. However, this trend decreases as slope height increases. Instead, at high slope heights, a greater reduction in slope angle is suggested if designing a slope with a low FS, compared with a slope where a greater FS is required.

Following Rock Mass A, the LE-based Excel-based solution from Carranza-Torres and Hormazábal (2018) can be used as a rapid means of comparison to the results from this analysis. Figure 11 illustrates that the results from the Slope Stability Curves, match the results from the LE-based solution for a drained analysis. This suggests that an LE-based solution for a weak (Mohr-Coulomb) rock mass can be used when the slope is fully drained. As with Rock Mass A, to consider the influence of groundwater an approach such as that presented in this paper, is necessary because there is no allowance for groundwater in the current Excel-based solution. It is intended that as part of a future study, Slope Stability Curves will be developed using IUCM in weak material, such as Rock Mass D. This will provide a further insight into the representation of complex behaviour, as was exhibited in Rock Mass A (Figure 6).

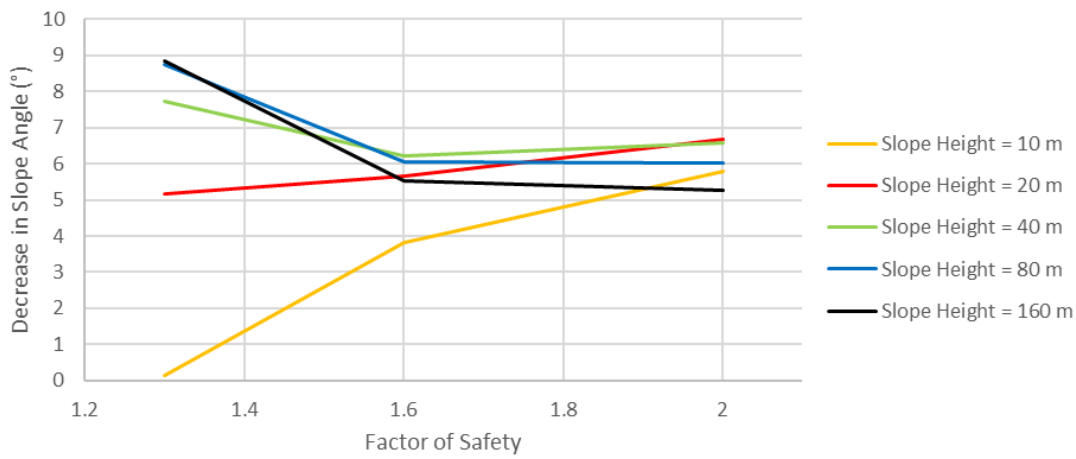


Figure 10. Decrease in slope angle suggested in Rock Mass D as a result of an increase in groundwater from fully drained (Chart 1) to Chart 2.

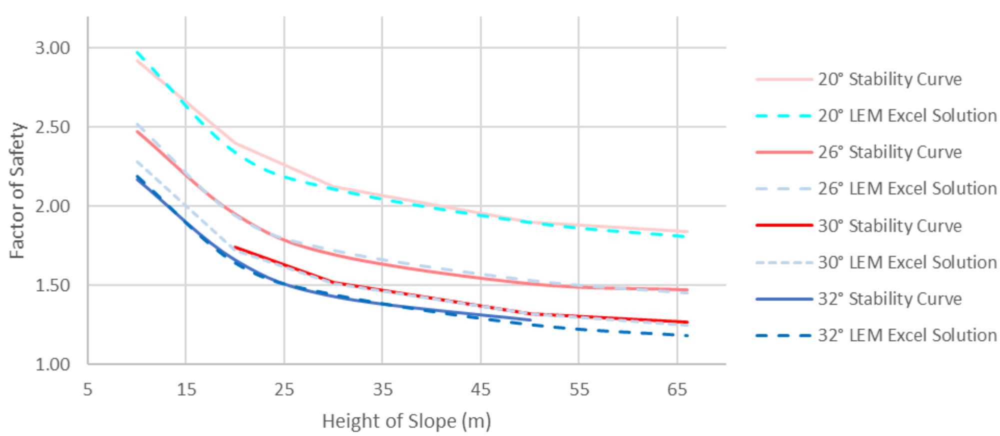


Figure 11. Comparison of Slope Stability curves for Rock Mass D (fully drained), with the LE-based Excel solution from Carranza-Torres and Hormazábal (2018).

## 5 Discussion

Slope Stability Curves have been introduced as a simple and easy-to-read slope height versus slope angle chart. The approach is intended to provide the means to develop a design chart for specified conditions. This can be used to as an initial guide or as a reference to study the influence of the geotechnical conditions, quantifying the change in slope angle to help direct where effort should be focussed at a project stage (definition of GSI, specific laboratory tests, and/or hydrogeology).

Continuing from the previous paper (Styles and Vakili, 2020), this paper focuses on two rock masses, one of which uses the Hoek-Brown strength criterion, and the other which uses a Mohr-Coulomb strength. The approach used to create a Slope Stability Curve, is described. The process involves using a matrix of slope geometries, to ensure that there are enough analyses to resolve the relationship between slope height and the FS, for a number of different slope angles.

The creation of Slope Stability Curves for rock masses with different strength criteria, provides confidence in the approach. Currently the method has been applied to rock slopes in the work to date, although it can also be applied to tipped material. This could provide additional safety in engineered materials, such as tailings embankments and waste dumps.

In addition to the two strength criteria, slope stability curves have been generated for different groundwater conditions, which shows the significant influence of groundwater. Furthermore, the results from the Slope Stability Curves have been interpretation to suggest:

- In general, both Rock Mass A and D, show that the influence of groundwater decreases as slope height and slope angle increases.
- There is a complex behaviour at low slope heights (<300 m and above a slope angle of 50°), where the reduction in FS due to groundwater is lower than would be anticipated.
- In high slopes with Rock Mass D, the amount that a slope angle should be reduced when groundwater is included, is greater at a low FS. This suggests the influence of groundwater is greater in higher slopes where a lower FS is required.

Comparisons have been made between the results from the Slope Stability Curves and a LE-based approach for drained conditions. The Slope Stability Curves match the results from the LE-based solution for Rock Mass D, whereas for Rock Mass A, which was analysed with the Hoek-Brown strength, there are some differences:

- The Slope Stability Curve suggests a slightly higher FS at lower slope heights, than the LE-based solution.
- At slope heights greater than approximately 500 m, the Slope Stability Curve suggests a significantly lower FS.

The reason for these differences is suggested to be due to complex behaviour. For instance, mechanical processes such as internal deformation and elevated stress in the toe of the slope, cannot be captured an LE-based approach.

Finally, it can be suggested that the 'D' factor is often used to weaken the rock mass, as opposed to analysing with a constitutive model that can directly address many of the shortcomings of the Hoek-Brown criterion, and explicitly include features such as anisotropy within the rock mass. The influence of anisotropy is briefly discussed, with an example, in which the FS decreases by ~1 once anisotropy was included. Future analyses will include both anisotropy and groundwater, to provide Slope Stability Curves that illustrate the critical nature of anisotropy, and the important of groundwater. With such potential reductions in FS, the slope height versus slope angle formulations that are presented on a ‘Slope Stability Curve’ may need to be reduced. As suggested by Read and Stacey (2009), the FS can be designed to be a as low as 1.16 for an inter-ramp slope, where there is a low consequence of failure. However, at such a low FS, the room for error is small; a 13% reduction in FS results in marginal stability. Therefore, it is critical that the influence of aspects that control the stability of a slope are quantified, using an approach such as Slope Stability Curves, minimising the risk during the planning phases of a mining project.

# 6 References


Carranza-Torres, C., Hormazabal, E. (2018). Computational tools for the determination of factor of safety and location of the critical circular failure surface for slopes in Mohr-Coulomb dry ground. *Proceedings of Slope Stability 2018 (congress)*. April 11-13 2018, Seville, Spain.

Carranza-Torres, C., Hormazábal, E. (2020). Computational tools for the estimation of Factor of Safety and location of the critical failure surface for slopes in rock masses that satisfy the Hoek–Brown failure criterion', in PM Dight (ed.), *Slope Stability 2020: Proceedings of the 2020 International Symposium on Slope Stability in Open Pit Mining and Civil Engineering*, Australian Centre for Geomechanics, Perth, pp. 1099-1122, https://doi.org/10.36487/ACG_repo/2025_73

Carter, T.G. (2018). Suggested Standards for Improving Structural Geological Definition for Open Pit Slope Design. *Final Papers - Slope Stability Symposium 2018*, Seville, Spain. 10-13 April 2018

Haines, A., Terbrugge, P.J. (1991). Preliminary estimate of rock slope stability using rock mass classification systems. 7th Congress of International Society of Rock Mechanics, Aachen, Germany, 16-20 September 1991

Hoek, E., Bray, J.W. (1981). *Rock Slope Engineering*, 3rd ed. The Institute of Mining and Metallurgy, London.

Li, A.J., Merifield, R.S., Lyami, A.V. (2008). Stability charts for rock slopes based on the Hoek–Brown failure criterion. International Journal of Rock Mechanics & Mining Sciences 45: 689–70.

Lorig, L. (2022). Overview of Slope Stability Analysis Methods. [Webinar]. [Online]. Itasca Consulting Group, Inc. [Accessed 1 June 2022]. Available from: https://www.itascacg.com/learning/webinars/overview-of-slope-stability-analysis-methods

Lucas, D.S., Vakili, A., Hutchinson, B.J. (2020) Slope design and control of rock fall hazards in a challenging structural setting at the Kanmantoo copper mine, South Australia. Slope Stability 2020, Perth, Australia, 12-14 May 2020.

Priest, S.D., Brown E.T. Probabilistic stability analysis of variable rock slopes. *Trans. Instn Min. Metall.* (Sect. A: Min. Industry), 92, 1983, A1- 12

Read, J., Stacey, P. (2009). *Guidelines for Open Pit Slope Design*. CSIRO Publishing, Collingwood.

Sun, C., Chai, J., Xua, Z., Qina, Y. Chen, X. (2016). Stability charts for rock mass slopes based on the Hoek-Brown strength reduction technique. Engineering Geology 214: 94–106.

Sjöberg, J. (1999). Analysis of Large Scale Rock Slopes. PhD thesis at Lulea University of Technology

Styles, T., Vakili, A. (2020). Slope angle versus slope height – the basis of an empirical tool for slope design within fractured rock masses using IUCM. ISRM International Symposium: Eurock 2020.

Vakili, A. (2016). An improved unified constitutive model for rock material and guidelines for its application in numerical modelling. Computers and Geotechnics 80: 261-282.

Vakili, A., Watson, J., Abedian, B., Styles, T. (2020). SlopeX – a Plug-in to Simplify and Fast-Track Advanced Numerical Modelling for Open Pit Applications. Slope Stability 2020, Perth, Australia, 12-14 May 2020.

Wei, Y., Liyan, W., Xing, Z., Tan Hanhua, T., Shu, P., Yanyu, X. Wei, W., Xiaoyun, S. Jiandong, N. (2021). A rapid stability charts analysis method for rock slopes based on Generalized Hoek-Brown criterion, All Earth, 33:1, 98-107.